AMERICAN JOURNAL OF PHYSIOLOGY
CELL PHYSIOLOGY

Am J Physiol Cell Physiol 320: C929–C942, 2021.
First published March 24, 2021; doi:10.1152/ajpcell.00508.2020

RESEARCH ARTICLE

Advances in Mitochondrial Biology: Mitochondria as Regulators of Health and Longevity

Mitochondrial functional resilience after TFAM ablation in the adult heart

Nasab Ghazal,[1] Jessica N. Peoples,[1] Tahmina A. Mohiuddin,[2] and Jennifer Q. Kwong[1]

[1]*Division of Pediatric Cardiology, Department of Pediatrics, Emory University School of Medicine and Children's Healthcare of Atlanta, Atlanta, Georgia and* [2]*Emory College of Arts and Sciences, Emory University, Atlanta, Georgia*

Abstract

The nuclear genome-encoded mitochondrial DNA (mtDNA) transcription factor A (TFAM) is indispensable for mitochondrial energy production in the developing and postnatal heart; a similar role for TFAM is inferred in adult heart. Here, we provide evidence that challenges this long-standing paradigm. Unexpectedly, conditional *Tfam* ablation in vivo in adult mouse cardiomyocytes resulted in a prolonged period of functional resilience characterized by preserved mtDNA content, mitochondrial function, and cardiac function, despite mitochondrial structural alterations and decreased transcript abundance. Remarkably, TFAM protein levels did not directly dictate mtDNA content in the adult heart, and mitochondrial translation was preserved with acute TFAM inactivation, suggesting maintenance of respiratory chain assembly/function. Long-term *Tfam* inactivation, however, downregulated the core mtDNA transcription and replication machinery, leading to mitochondrial dysfunction and cardiomyopathy. Collectively, in contrast to the developing heart, these data reveal a striking resilience of the differentiated adult heart to acute insults to mtDNA regulation.

cardiomyocytes; heart; mitochondria; mtDNA; TFAM

INTRODUCTION

Mitochondria are critical to fuel cardiac contraction. These organelles occupy ~30% of the cardiomyocyte by volume and provide ~90% of the ATP that is used on a beat-to-beat basis (1, 2). Defects in mitochondrial energy production underlie many diseases that affect the heart, ranging from primary mitochondrial cardiomyopathies due to defects in the oxidative phosphorylation (OXPHOS) system, to heart failure and aging (3–6). Dissecting mechanisms regulating mitochondrial energy production systems therefore affords critical knowledge to understand basic cardiac physiology.

Mitochondria are under the dual control of the nuclear genome [nuclear DNA (nDNA)] and the mitochondrial genome (mtDNA). Although most of the ~1,100 proteins of the mammalian mitochondrial proteome are specified by nDNA (7), mtDNA specifies 13 essential subunits of the respiratory chain, alongside two ribosomal RNAs (rRNAs) and 22 transfer RNAs (tRNAs) that are required for mtDNA protein translation (8). The mtDNA is distinct from and regulated independently of the nDNA, but shares similar organization into discrete DNA-protein structures, called nucleoids (9).

MtDNA nucleoids encompass proteins involved in mtDNA maintenance, replication, transcription, and translation (10–12). A key protein within the mtDNA nucleoid structure is the mitochondrial transcription factor A (TFAM), an nDNA-encoded mtDNA-binding protein with established roles in mtDNA packaging (13–15), transcription (16, 17), replication (18), and copy number maintenance (19, 20). In vivo studies confirm these critical roles of TFAM: systemic inactivation of murine TFAM causes early embryonic lethality [by *embryonic day* (*E*) *10.5*] that is accompanied by mtDNA depletion and reduced mitochondria-encoded respiratory chain complex activity (21).

The essential nature of TFAM in vivo is mirrored in the developing embryonic and postnatal heart. Inactivation of *Tfam* in the mouse embryonic heart at *E7.5* using the *Nkx2.5*-Cre recombinase results in lethality by *E15.5*, with the embryonic hearts marked by myocardial wall thinning (22). *Tfam* deletion in the skeletal muscle and heart mediated by the muscle creatinine kinase promoter-driven Cre (*Ckmm*-Cre), which initiates deletion at *E13*, triggers development of dilated cardiomyopathy with atrioventricular conduction blocks and death by 2 to 4 wk postnatal age (23). This dilated cardiomyopathy phenotype and severely blunted survival can be recapitulated with cardiomyocyte-specific *Tfam* inactivation in the postnatal heart using Cre under the control of the α myosin heavy chain promoter (αMHC-Cre), which induces robust gene deletion in the postnatal ventricular cardiomyocytes (24, 25). Unifying these existing mouse models, TFAM ablation early in life causes severe mtDNA copy number reduction, impaired mtDNA

Correspondence: J. Q. Kwong (jennifer.kwong@emory.edu).
Submitted 29 October 2020 / Revised 22 March 2021 / Accepted 22 March 2021

gene expression, reduced mitochondrial respiratory chain complex assembly, respiratory chain dysfunction, and abnormal mitochondrial ultrastructure (22–25).

These existing models define the importance of proper mtDNA regulation in the developing heart, which is a period of active cardiomyocyte growth and proliferation (26). The role of mtDNA regulation in the adult heart has been inferred from such findings. However, the heart is a terminally differentiated tissue. The transition from the postnatal heart at birth to a fully developed adult organ is marked by multiple rounds of early cardiomyocyte proliferation followed by hypertrophic growth (26). During this period, cardiac mitochondria also undergo a profound structural and functional maturation, with the fragmented mitochondria of embryonic and early postnatal cardiomyocytes developing into the interconnected network of adult cardiomyocytes (27). This transition is marked by increase mitochondrial biogenesis and a metabolic shift toward β-oxidation (27, 28). The fully differentiated adult heart could therefore have different needs for mtDNA maintenance, but this question has not been investigated.

In this study, we investigated the function of the mtDNA maintenance machinery in the adult heart by engineering a mouse model with tamoxifen-inducible cardiomyocyte-specific deletion of *Tfam* ($Tfam^{fl/flxMCM}$ mice). Surprisingly, we found that TFAM does not determine mtDNA copy number in the adult heart and that the adult heart displays a remarkable functional resilience in response to TFAM ablation, where cardiac structure, function, and mitochondrial energetics can be maintained. Moreover, mitochondrial function appears to be sustained by preserved mitochondrial protein translation. Finally, although long-term (>5 mo) TFAM ablation causes dilated cardiomyopathy marked by mtDNA depletion as well as reduced mtDNA gene expression, these phenotypes may be potentiated by a coordinated downregulation of the mitochondrial transcription and replication machinery. Collectively, our data demonstrate differing responses to defects in the mtDNA maintenance and expression machinery between developing/postnatal and adult hearts, and point to preserved mitochondrial translation as a potential pathway that confers resistance to mitochondrial insults in the adult myocardium.

MATERIALS AND METHODS

Animals

$Tfam^{fl/fl}$ loxP-targeted mice were obtained from The Jackson Laboratories (Stock No. 026123) and were generated as described in Larsson et al. (21). $Tfam^{fl/flxCre}$ mice were generated by crossing $Tfam^{fl/fl}$ mice to animals expressing a Cre recombinase under the control of the α myosin heavy chain promoter (Cre) (29). The $Tfam^{fl/flxMCM}$ model of tamoxifen-regulated cardiac *Tfam* ablation was constructed by crossing $Tfam^{fl/fl}$ mice to animals expressing a tamoxifen inducible Cre recombinase under the control of the cardiomyocyte specific α-myosin heavy chain promoter (MCM) (30). For this study, animals of both sexes were used. *Tfam* deletion was induced in 8-wk-old $Tfam^{fl/flxMCM}$ animals by intraperitoneal injections of tamoxifen (25 mg/kg for 5 consecutive days). Control animals, harboring either the *Tfam* targeted locus ($Tfam^{fl/fl}$) or MCM transgene alone, were subjected to the same tamoxifen-dosing regimen. Experiments were conducted on mice at 2, 13, 20, and 32 wk following tamoxifen administration as indicated. For euthanasia of animals for collection of heart tissue in our study, animals were anesthetized with isoflurane followed by cervical dislocation. All animal experiments were approved and performed in accordance to Emory University's Institutional Animal Care and Use Committee (IACUC).

Echocardiography

Mice were anesthetized with isoflurane (1.5%) with body temperature maintained at 37°C and measurements were performed using a Vevo 2100 Imaging System (Visual Sonics) equipped with a MS-400 transducer. M-mode measurements were taken of the parasternal short axis view. Systolic and diastolic ventricular chamber dimensions, ventricular wall and septal thicknesses were assessed, and fractional shortening was calculated using the VevoLab software.

Electrophoresis and Immunoblotting

For Western blots, total protein extracts were prepared from hearts solubilized in radioimmunoprecipitation assay (RIPA) buffer supplemented with a combined protease and phosphatase inhibitor cocktail (Thermo Fisher Scientific). Mitochondrial protein extracts were prepared by solubilizing isolated cardiac mitochondria in the same RIPA buffer. For Western blotting of adult cardiomyocytes isolated from hearts by Langendorff perfusion with liberase blendzyme (0.25 mg/mL) and trypsin (0.14 mg/mL) in Krebs–Henseleit buffer as previously described (31). Proteins were reduced and denatured in Laemmli buffer, resolved on 10% SDS-PAGE gels, transferred to PVDF membranes, immunodetected with antibodies, and imaged using a ChemiDoc system (BioRad). Primary antibodies used in the study were: anti-TFAM (Abcam, ab131607, 1:1,000), anti-Porin (Abcam, ab14734, 1:1,000), anti-ND1 (Proteintech, 19703-1-AP, 1:1,000), anti-COXII (Proteintech, 55070-1-AP, 1:1,000), OXPHOS Blue Native WB Antibody Cocktail (Abcam, ab110412, 1:500; this cocktail contains antibodies against SDHA ATP5A, UQCRC2, NDUFA9, and COXIV), and anti-GAPDH (Fitzgerald, 10 R-G109A, 1:10,000). The secondary antibodies use were alkaline phosphatase-linked goat anti-rabbit IgG (Cell Signaling Technologies No. 7054) and alkaline phosphatase-linked goat anti-mouse IgG (Cell Signaling Technologies No. 7056).

mtDNA Copy Number Analysis

Total DNA was prepared from snap-frozen heart tissue using the DNAeasy Kit (Qiagen). Quantification of relative mtDNA copy number was conducted by measuring the mtDNA/nDNA ratio using quantitative PCR. Primers for mouse mtDNA (Forward, CTAGAAACCCCGAAACCAAA; Reverse, CCAGCTATCACCAAGCTCGT) and the β-2-microglobulin nuclear DNA (Forward, ATGGGAAGCCGAACATACTG; Reverse CAGTCTCAGTGGGGGTGAAT) were used as previously described (32). The qPCR assay was performed using the LightCycler 480 SYBR Green I Master (Roche) using Applied Biosystems QuantStudio 6 Flex Real-Time

PCR System. Relative mtDNA copy number was calculated using the ΔΔC(t) method.

RT-PCR

Total RNA was extracted from heart tissue using the RNeasy Fibrous Tissue Mini Kit (Qiagen) and cDNA was generated using the High Capacity cDNA Reverse Transcription Kit (Applied Biosystems). Real-time PCR (RT-PCR) was performed on a QuantStudio 6 Flex Real-Time PCR System (Applied Biosystems) with LightCycler 480 SYBR Green I Master (Roche). Primer sequences were obtained from PrimerBank (33). ΔΔC(t) was used to quantify the fold change of the target genes. The primer sets used were: *Mtatp6* (Forward, CCTTCCACAAGGAACTCCAATTTCAC; Reverse, CTAGAGTAGCTCCTCCGATTAGGTG), *Mtco1* (Forward, GCAGGAGCATCAGTAGACCTAAC; Reverse, GGAGTTTGATACTGTGTTATGGCTGG), *Mtcytb* (Forward, CTACTGTTCGCAGTCATAGCCAC; Reverse, CCAATATATGGGATGGCTGATAGGAG), *Mtnd5* (Forward, GGCCTATTAATCGCAGCTACAGG; Reverse, GTAGTAGTGCTGAAACTGGTGTAGG) (25), *Mtnd6* (Forward, ATGTTGGAAGGAGGGATTGGG; Reverse, TACCCGCAAACAAAGATCACC) (34), *Polrmt* PrimerBank ID 27369780a1 (Forward, GGCCCATCTTGCATTCTAGGG; Reverse, CAGGCAACGGCTCTATATTGAAG), *Tfb2m* PrimerBank ID 6680223a1 (Forward, CCGCGTGCTGAGCATAAATC; Reverse, ACTGCACTAAGAGGTCCTGTG), *Tefm* PrimerBank ID 18044017a1 (Forward, CAACAAATGAGATGTGGCGATCA; Reverse, ACGAGCTTCTTACCAGCTATGA), *Polg* PrimerBank ID 8567392a1 (Forward, GAGCCTGCCTTACTTGGAGG; Reverse, GGCTGCACCAGGAATACCA), *Pnpt1* PrimerBank ID 12835817a1(Forward, AATCGGGCACTCAGCTATTTG; Reverse CAGGTCTACAGTCACCGCTC), *Supv3l1* PrimerBank ID 31088872a1 (Forward, GTGCAGCTCATGTGGACGATT; Reverse, GGGTGGTATCCTCAAGTCACTG) *Twnk* (Forward, GCCACGTGACTCTGGTCATTC; Reverse, CCATCAAAGCGATTCTTGGACA) (20), *Rps20* (Forward, AACAAGTCGGTCAGGAAGC; Reverse, TCCGCACAAACCTTCTCC), *Ndufa9* PrimerBank ID 13384720a1 (Forward, GTCCGCTTTCGGGTTGTTAGA; Reverse, CCTCCTTTCCCGTGAGGTA), *Sdha* PrimerBank ID 15030102a1 (Forward, GGAACACTCCAAAAACAGACCT; Reverse, CCACCACTGGGTATTGAGTAGAA), *Cox4i1* PrimerBank ID 6753498a1 (Forward, ATTGGCAAGAGAGCCATTTCTAC; Reverse, CACGCCGATCAGCGTAAGT), *Myh6* PrimerBank ID 6754774a1 (Forward, GCCCAGTACCTCCGAAAGTC; Reverse, GCCTTAACATACTCCTCCTTGTC), *Nppa* PrimerBank ID 387099a1 (Forward, GCTTCCAGGCCATATTGGAG; Reverse, GGGGGCATGACCTCATCTT), *Nppb* Primerbank ID 6679112a1 (Forward, GAGGTCACTCCTATCCTCTGG; Reverse, GCCATTTCCTCCGACTTTTCTC), and *Pgc1α* PrimerBank ID 6679433a1 (Forward TATGGAGTGACATAGAGTGTGCT, Reverse, CCACTTCAATCCACCCAGAAAG).

Transmission Electron Microscopy

Mouse heart samples were fixed in 2.5% glutaraldehyde in 0.1 M cacodylate buffer (pH 7.4), postfixed in 1% osmium tetroxide, and embedded in epoxy resin. Ultrathin sections (80–90 nm) were cut with a Leica EM CU6 microtome and counterstained with uranyl acetate and lead citrate. Sections were imaged on a JEOL JEM-1400 transmission electron microscope (Tokyo, Japan) equipped with a Gatan US1000 CCD camera (Pleasanton, CA).

Mitochondrial Oxygen Consumption

Cardiac mitochondria were prepared by differential centrifugation as previously described (35). Oxygen consumption was measured on isolated heart mitochondria using an Oxytherm System (Hansatech) as described (36). Briefly, mitochondria were suspended in respiration buffer containing 120 mM KCl, 5 mM MOPS, 0.1 mM EGTA, 5 mM KH_2PO_4, 0.2% BSA, 10 mM glutamate, and 2 mM malate. Basal ADP-stimulated respiration was initiated with the addition of 0.5 mM ADP, uncoupled respiration was induced with the addition of 5 μM FCCP, and nonmitochondrial oxygen consumption was assessed with the addition of KCN. Basal and maximal uncoupled mitochondrial oxygen consumption rates were obtained by subtracting KCN-nonmitochondrial respiration, followed by normalization to protein concentration.

Histology

Hearts were fixed in 10% formalin and embedded in paraffin. Paraffin-embedded tissues were sectioned (7 μm) and stained with hematoxylin and eosin (H&E) and Masson's trichrome. Images were captured using a Nanozoomer 2.0-HT whole slide scanner (Hamamatsu). Myocyte cross-sectional area was quantified on images of H&E stained sections using NIH Image J software.

In Organello Translation Assay

In organello translation assays were performed with a modified protocol based on Fernandez-Silva et al. (37). Briefly, cardiac mitochondria were suspended in mitochondrial isolation buffer (25 mM sucrose, 75 mM sorbitol, 100 mM KCl, 1 mM $MgCl_2$, 0.05 mM EDTA, 10 mM TrisHCl, and 10 mM K_2HPO_4, pH 7.4) supplemented with 10 mM glutamate, 2.5 mM malate, 1 mM ADP, 1 mg/mL fatty acid-free bovine serum albumin, and 100 μg/mL cycloheximide and incubated with 100 μM L-azidohomoalanine (AHA; Click Chemistry Tools) and 10 μM methionine-free amino acid mixture (Promega). The Click-iT reaction was performed with the Click-&-Go Protein Reaction Buffer Kit (Click Chemistry Tools) and AF488 alkyne (Click Chemistry Tools) according to the manufacturer's instructions. Proteins were resolved by SDS-PAGE and imaged using a ChemiDoc MP Imaging System (BioRad).

BN-PAGE

Blue-native polyacrylamide gel electrophoresis (BN-PAGE) followed by immunoblotting for respiratory complexes was performed as described previously (38, 39). Briefly, isolated heart mitochondria were solubilized with digitonin [Sigma Aldrich, 6 g/g digitonin/protein ratio) and resolved on a 4%–12% Bis-Tris polyacrylamide gradient gel (Genscript)]. Proteins were transferred to PVDF membranes and immunodetection of respiratory chain complexes was performed using the Total OXPHOS Blue Native WB Antibody Cocktail (Abcam, ab110412, 1:250). The membrane was imaged using a Chemidoc XRS + System (BioRad).

Statistics

All results are presented as means ± SE. Statistical significance between two groups was determined by Student's t test, with $P < 0.05$ considered significant.

Study Approval

All experiments involving mice were approved by the IACUC at Emory University, Approval No. PROTO201700174.

RESULTS

Cardiomyocyte-Restricted Ablation of TFAM in the Developing Early Postnatal versus Adult Mouse Heart

To dissect effects of mtDNA machinery disruptions in the mouse heart, we compared two models of cardiomyocyte-specific ablation of TFAM. For postnatal deletion of TFAM in the heart, we crossed *Tfam* loxP-targeted animals ($Tfam^{fl/fl}$) (21) with mice expressing a Cre recombinase under the control of the cardiomyocyte-specific αMHC promoter (Cre; $Tfam^{fl/flxCre}$, Fig. 1*A*) (29). To achieve deletion of TFAM in the adult heart, we crossed $Tfam^{fl/fl}$ mice with mice harboring a tamoxifen-inducible αMHC-driven Cre (MCM; $Tfam^{fl/flxMCM}$, Fig. 1*E*) (30). Cardiomyocyte-specific TFAM deletion was induced by systemic tamoxifen administration to adult (8-wk-old) $Tfam^{fl/flxMCM}$ experimental mice, with $Tfam^{fl/fl}$ mice serving as controls (tamoxifen 25 mg/kg/day for 5 days, Fig. 1*F*). Both the constitutive postnatal αMHC-Cre (evaluated at 15 days of age) as well as the inducible adult MCM systems (evaluated 2 wk post-tamoxifen administration, Fig. 1*B*) resulted in a significant reduction in TFAM protein expression in the heart as assessed by immunoblotting (Fig. 1*G*). TFAM protein levels were not further reduced in $Tfam^{fl/flxMCM}$ versus $Tfam^{fl/fl}$ cardiac tissue by extending the time between tamoxifen dosing and immunoblot analysis of protein expression (Supplemental Fig. S1; all Supplemental Material is available at https://doi.org/10.6084/m9.figshare.14153687), suggesting that 2 wk following the tamoxifen-initiated Cre recombination maximally decreases TFAM in the heart.

Acute Loss of TFAM Has No Structural or Functional Impact on the Adult Mouse Heart

TFAM deletion systemically or in the embryonic heart causes embryonic lethality, whereas deletion in either developing striated muscle or cardiomyocytes results in mitochondrial cardiomyopathy and early lethality (22, 24, 25). In line with these studies, we found that $Tfam^{fl/flxCre}$ mice exhibited reduced survival, with no animals surviving longer than 74 days of age (Fig. 1*C*), as well as a significant increase in heart weight/body weight ratios as compared with $Tfam^{fl/fl}$ controls at 60 days of age (Fig. 1*D*). Thus, unsurprisingly, postnatal TFAM deletion in the heart induces pathological cardiac remodeling and hypertrophy.

To investigate the functional consequences of TFAM ablation in the adult heart, gravimetric and echocardiographic analyses were initially conducted on TFAM-deleted ($Tfam^{fl/flxMCM}$) and control ($Tfam^{fl/fl}$) mice 2 wk after tamoxifen administration. At this acute time point, despite the significant decrease in TFAM protein levels in cardiomyocytes (Fig. 1*G*), no changes were detected in gravimetric or echocardiographic parameters (Fig. 1, *H–J*). Strikingly, cardiac dimensions and function (heart weight/body weight ratios, left ventricular interior dimensions, fractional shortening) remained unaltered even at 20 wk after tamoxifen dosing (Fig. 1, *K–M*). Together, these data suggest that, unlike in the postnatal developing heart, in the adult heart following acute loss, TFAM is dispensable for structural or functional maintenance of the heart.

TFAM-Deleted Animals Develop Cardiomyopathy with Aging

The strikingly normal cardiac structure and function following acute loss of TFAM in adult hearts prompted us to investigate the effects of prolonged TFAM loss. At 32 wk after tamoxifen dosing (Fig. 2*A*), histological analyses of heart sections revealed extensive inflammatory cell infiltrates (Fig. 2*B*), significantly elevated cardiomyocyte cross-sectional area (Fig. 2*C*), and increased fibrosis (Fig. 2*D*) in $Tfam^{fl/flxMCM}$ mice as compared with $Tfam^{fl/fl}$ controls. In addition, $Tfam^{fl/flxMCM}$ mice developed elevated heart weight/body weight and lung weight/body weight ratios as compared with $Tfam^{fl/fl}$ controls (Fig. 2, *E–F*), indicating cardiac hypertrophy and pulmonary edema. Echocardiographic analyses further showed that TFAM-deleted animals had increased left ventricular dimensions at diastole (LVIDd; Fig. 2*G*) and decreased fractional shortening (FS; Fig. 2*H*), indicating ventricular dilation and impaired cardiac performance. In addition, real time PCR (RT-PCR) analyses of established hypertrophy markers revealed an increase in *Nppa* and *Nppb* expression together with a decrease in *Myh6* expression (Fig. 2, *I–K*), indicating that TFAM deletion-induced cardiomyopathy is associated with reexpression of the fetal cardiac gene program. Collectively, these data show that $Tfam^{fl/flxMCM}$ mice develop dilated cardiomyopathy with aging.

Mitochondrial Structural Remodeling Is an Early Response to TFAM Deletion

To understand how TFAM ablation affects mitochondria in the adult heart, we examined cardiac respiratory chain function. Respirometry was conducted on mitochondria isolated from $Tfam^{fl/flxMCM}$ and $Tfam^{fl/fl}$ hearts at the 2-, 20-, and 32-wk posttamoxifen time points (Fig. 3, *A–C*). Consistent with our observations of maintained cardiac structure and function upon acute TFAM deletion (Fig. 1, *H–M*), no significant differences were observed in basal or maximal oxygen consumption rates in TFAM-deleted versus control mitochondria at either the 2- or 20-wk deletion time points (Fig. 3, *A–B*). In contrast, TFAM deletion-induced deficits in respiration were observed at 32 wk of TFAM ablation (Fig. 3*C*). Thus, mitochondrial function can be maintained in the acute absence of TFAM, but long-term TFAM deletion induces respiratory defects.

To determine the effects of TFAM loss on mitochondrial organization, transmission electron microscopy was conducted to examine mitochondrial ultrastructure. Remarkably, TFAM deletion disrupted cardiac mitochondrial morphology as early as 20 wk after tamoxifen administration (Fig. 3, *D–E*, Supplemental Fig. S2), and TFAM deletion-induced alterations in mitochondrial organization (20 wk; Fig. 3*D*, Supplemental

Fig. S2*A*) occurred before the onset of respiratory chain dysfunction (observed at 32 wk, Fig. 3*C*). Together, these observations support a model whereby TFAM participates in the maintenance of cardiac mitochondrial organization, and this structural role of TFAM appears distinct from the effects of TFAM loss on mitochondrial energetics.

TFAM Deletion-Induced mtDNA Transcription Defects Precede mtDNA Depletion

Deletion of TFAM in vitro, as well as in the contexts of embryonic and early postnatal cardiac development, causes respiratory chain dysfunction due to mtDNA depletion,

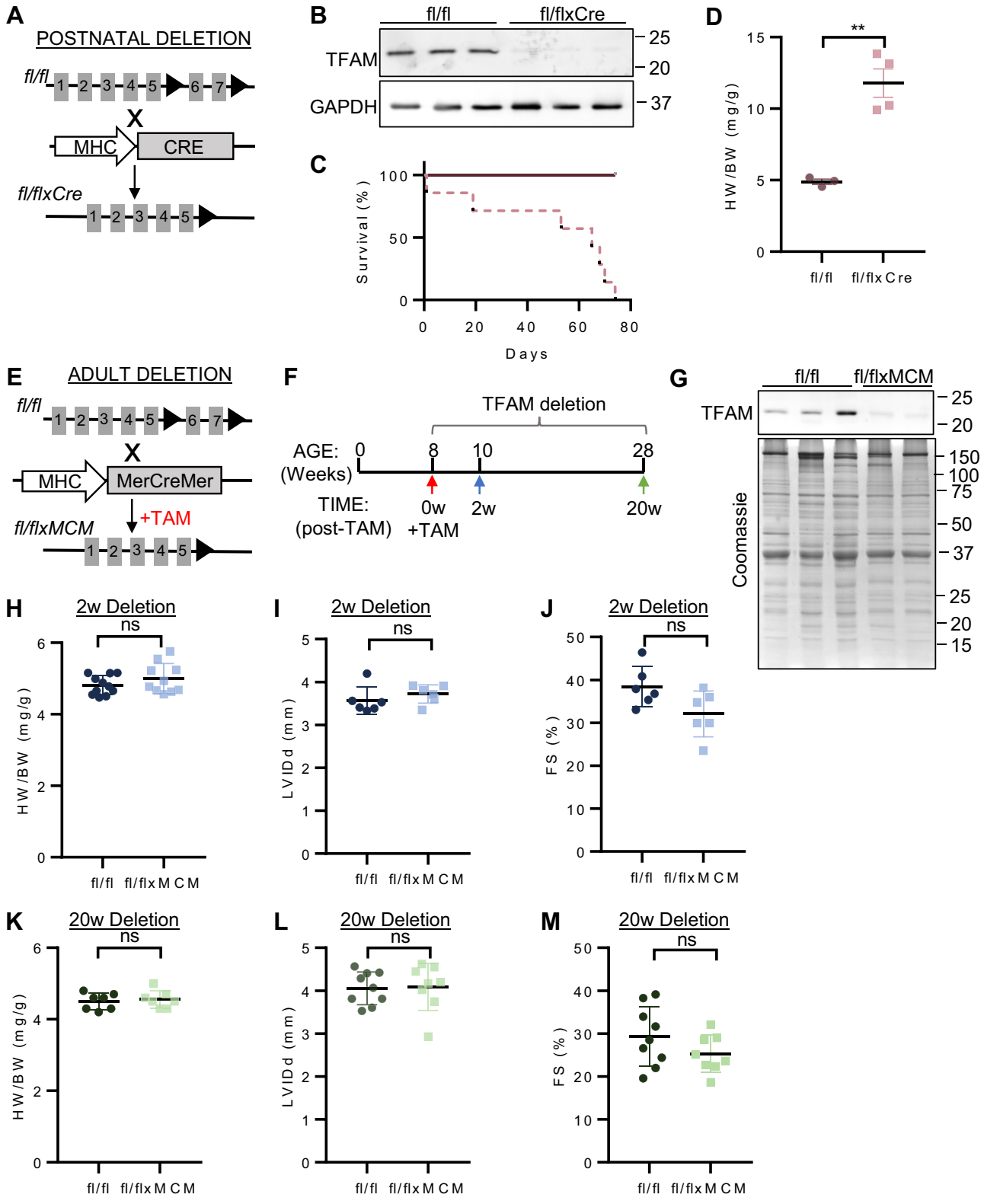

impaired transcription, and a decline in respiratory chain complex expression and assembly (21, 23–25). Our observation that adult heart mitochondria display preserved respiration (Fig. 3, *A* and *B*) for months in the absence of TFAM protein was therefore unexpected. Given this surprising finding, we examined mtDNA content and mtDNA transcript levels in $Tfam^{fl/flxMCM}$ versus $Tfam^{fl/fl}$ hearts. Steady-state levels of representative mitochondrial transcripts spanning different mtDNA-encoded respiratory chain complexes (*Mtnd5* and *Mtnd6* for complex I, *Mtcytb* for complex III, *Mtco1* for complex IV, and *Mtatp6* for complex V) were assessed by RT-PCR. TFAM deletion in the heart resulted in a progressive decline in mtDNA-encoded transcripts (Fig. 4, *A*–*C*), with decreased abundance of some transcripts (*Mtnd5*) observed as early as 2 wk posttamoxifen administration (Fig. 4*A*). This alteration suggests that loss of TFAM induces an immediate decline in mtDNA transcription. Moreover, transcript expression of the mitochondrial RNA degradosome constituents *Pnpt1* (mitochondrial polyribonucleotide nucleotidyltransferase 1) and *Supv3l1* (mitochondrial ATP-dependent RNA helicase), which participate in mitochondrial RNA degradation (40), were unchanged at the 2- and 20-weeks posttamoxifen times points (Supplemental Fig. S3), suggesting that changes in mitochondrial RNA half-life do not contribute to TFAM deletion-induced decrease in mtDNA transcript levels.

To evaluate the impact of TFAM deletion on mtDNA content, mtDNA/nDNA ratios were measured from total DNA isolated from hearts of $Tfam^{fl/flxMCM}$ versus $Tfam^{fl/fl}$. Surprisingly, decreased mtDNA/nDNA ratio was observed only in $Tfam^{fl/flxMCM}$ hearts 32 wk following tamoxifen administration (Fig. 4, *D*–*F*), suggesting that mtDNA content can be maintained for months in the absence of TFAM. Collectively, these data suggest that in the adult heart, there is a differential requirement for TFAM's functions in mtDNA maintenance versus transcription, and these functions can be differentiated; there may be an ongoing requirement for TFAM in transcription, but TFAM's roles in mtDNA maintenance and replication may only be appreciable with long-term deletion.

Mitochondrial Translation and Respiratory Chain Protein Levels Are Maintained during Functional Resilience

Given that the early phase of TFAM deletion (between 2 and 20 wk posttamoxifen, a period that we have termed "functional resilience") is marked by preserved mitochondrial function despite decreases in transcription, we next asked if mitochondrial protein translation could be maintained despite decreases in transcription. In organello translation assays were performed on cardiac mitochondria isolated from mice ($Tfam^{fl/fl}$ and $Tfam^{fl/flxMCM}$) 13 wk posttamoxifen. Quantification of the levels of $Tfam^{fl/flxMCM}$ versus $Tfam^{fl/fl}$ mitochondrial protein synthesis products revealed no differences between the two groups (Fig. 5, *A* and *B*). To further examine the consequences of TFAM ablation on respiratory chain complex assembly during this acute/early deletion phase, we performed blue-native gel electrophoresis of $Tfam^{fl/fl}$ and $Tfam^{fl/flxMCM}$ mitochondria. Consistent with our observations of unaltered translation, no differences in assembled respiratory chain complex abundance were detected between the two groups (Fig. 5, *C* and *D*). Corresponding to the sustained levels of assembled respiratory chain complexes during functional resilience, Western blot analyses for individual respiratory chain complex subunits also revealed no changes following TFAM deletion (Fig. 5*E*).

Because the respiratory chain requires the coordinated assembly of mtDNA and nDNA encoded proteins and changes in mitochondrial function/respiration may impact the expression of nDNA-encoded mitochondrial proteins, we further investigated the effects of TFAM deletion on transcript levels and protein expression of representative nDNA mitochondrial respiratory chain subunits over the course of development of TFAM deletion-induced cardiomyopathy (2, 20, and 32 wk of deletion). As anticipated, RT-PCR analyses of representative nDNA-encoded respiratory chain transcripts (*Ndufa9*, *Sdha*, *Cox4il*) were unchanged in $Tfam^{fl/flxMCM}$ versus $Tfam^{fl/fl}$ hearts 2 wk posttamoxifen (Supplemental Fig. S4*A*). By 20 wk posttamoxifen (the end of our functional resilience window), there was a slight but significant reduction in these transcripts in $Tfam^{fl/flxMCM}$ versus $Tfam^{fl/fl}$ hearts (Supplemental Fig. S4*B*) that was further magnified by the 32-wk posttamoxifen time point (Supplemental Fig. S4*C*), suggesting that the TFAM deletion-induced defects in mtDNA transcription were followed by a coordinate downregulation of transcription of nDNA-encoded respiratory chain components. To understand the mechanisms controlling the decrease in nDNA-encoded respiratory chain components, we examined the expression of PCG1α (peroxisome proliferator-activated receptor-γ coactivator-1α), a transcriptional co-activator that controls the transcription of cellular energy metabolism associated genes including nDNA-encoded respiratory chain subunits (41) by RT-PCR. We found that PGC1α transcript levels mirrored the expression profile of nDNA-encoded mitochondrial respiratory chain subunits, where PGC1α expression was unchanged at the 2-wk posttamoxifen deletion time point, but reduced at 20 and 32 wk of deletion

Figure 1. Acute loss of mitochondrial transcription factor A (TFAM) has no structural or functional impact on the adult mouse heart. *A*: generation of the $Tfam^{fl/flxCre}$ model of TFAM deletion in postnatal cardiomyocytes. *Tfam* loxP (red triangles) targeted mice (fl/fl) crossed to mice expressing an αMHC promoter-driven Cre recombinase. *B*: Western blot of TFAM expression in total cardiac protein of the indicated genotypes at 15 days of age. GAPDH was used as a loading control. *C*: Kaplan–Meier survival curve ($n = 7$/group). *D*: heart weight to body weight ratio (HW/BW) of the indicated groups of mice at 60 days of age ($n = 3$ fl/fl and $n = 4$ fl/flxMCM mice). $^{**}P < 0.01$ vs. fl/fl mice. *E*: generation of the $Tfam^{fl/flxMCM}$ mice. $Tfam^{fl/fl}$ mice were crossed to αMHC-MerCreMer (MCM) transgenic mice, which express a tamoxifen (TAM) inducible Cre under the control of the αMHC promoter. *F*: tamoxifen dosing regimen (25 mg/kg/day ip for 5 days) and experimental time course for acute TFAM deletion (2 and 20 wk posttamoxifen). *G*: Western blot of TFAM expression in adult cardiomyocytes isolated from $Tfam^{fl/fl}$ and $Tfam^{fl/flxMCM}$ animals at the 2 wk post-tamoxifen time point. HW/BW ($n = 11$ fl/fl and $n = 10$ fl/flxMCM mice) (*H*), left ventricular interior dimension in diastole (LVIDd; $n = 6$ fl/fl and $n = 6$ fl/flxMCM mice) (*I*), and fractional shortening (FS; $n = 6$ fl/fl and $n = 6$ fl/flxMCM mice) (*J*) as assessed by echocardiography at 2 wk posttamoxifen administration. HW/BW ($n = 7$ fl/fl and $n = 7$ fl/flxMCM mice) (*K*), LVIDd ($n = 9$ fl/fl and $n = 8$ fl/flxMCM mice) (*L*), and FS ($n = 9$ fl/fl and $n = 8$ fl/flxMCM mice) (*M*) as assessed by echocardiography at 20 wk posttamoxifen administration. All values reported as means ± SE. Student's *t* test was used for statistical analysis. $P < 0.05$ was considered significant.

(Supplemental Fig. S5). Surprisingly, however, Western blot analyses representative nDNA-encoded respiratory chain protein subunits revealed that protein levels were unaltered throughout the course of TFAM-induced cardiomyopathy (Supplemental Fig. S6), suggesting that nDNA-encoded proteins of the respiratory chain may be long-lived and that TFAM deletion-responsive reduction in PCG1α and inhibition of nDNA respiratory chain complex subunit transcription is

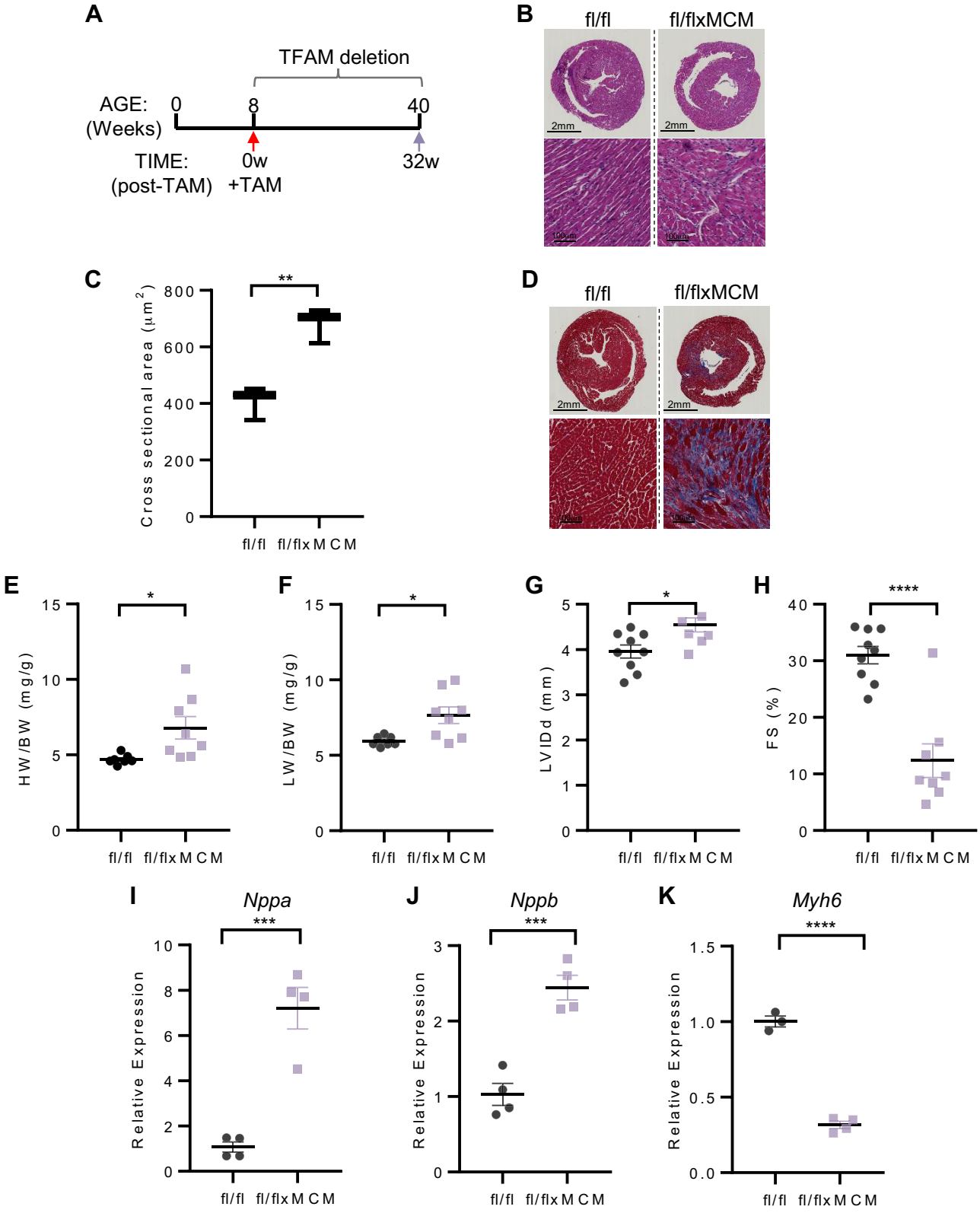

not a major contributor to the onset of TFAM-deletion induced cardiac disease.

Collectively, these data indicate that, despite TFAM deletion-induced reduction steady-state mtDNA and nDNA-encoded transcripts of respiratory chain complex constituents, $Tfam^{fl/flxMCM}$ myocytes can preserve an assembled respiratory chain by sustaining normal levels of mitochondrial protein synthesis and nDNA-encoded respiratory chain subunit levels. The findings suggest a possible mechanism whereby mitochondrial function can be preserved despite TFAM-deletion induced impairments in mtDNA and nDNA respiratory chain-associated gene expression in the fully differentiated cardiomyocyte.

Prolonged TFAM Loss Causes a Coordinated Downregulation of Mitochondrial Transcription and Replication Machinery

Having established that translation is maintained in mitochondria in the absence of TFAM, possibly serving to maintain mitochondrial function (Fig. 3, *A* and *B*), we next investigated if additional factors ultimately contribute to the reduced mtDNA content (Fig. 4*F*) and transcription (Fig. 4*C*) as well as functional decline (Fig. 3*C*) observed with prolonged TFAM ablation. Specifically, we focused on the mitochondrial transcription and replication machinery. Together with TFAM, mitochondrial transcription requires the coordinated actions of mitochondrial RNA polymerase (POLRMT), mitochondrial transcription factor B2 (TFB2M), and mitochondrial transcription elongation factor (TEFM) (42). We evaluated transcript expression of these mtDNA transcription regulators by RT-PCR. Although *Polrmt*, *Tfb2m*, and *Tefm* transcript levels were unchanged in $Tfam^{fl/fl}$ versus $Tfam^{fl/flxMCM}$ during functional resilience (2- and 20-wk posttamoxifen time points; Supplemental Figs. S7 and S8), these transcripts were significantly downregulated at 32-wk posttamoxifen (Fig. 6*A*). Furthermore, transcript abundance of the helicase Twinkle (*Twnk*) and the mitochondrial polymerase gamma (*Polg*) significantly declined in $Tfam^{fl/flxMCM}$ hearts compared with $Tfam^{fl/fl}$ controls (Fig. 6*B*). Taken together, prolonged loss of TFAM causes a loss of the core components of mtDNA transcription and replication machinery, and suppression of these systems likely contributes to the severe mitochondrial defects and cardiomyopathy (Fig. 2) observed with long-term TFAM deletion.

DISCUSSION

We conducted the first study of the functional consequences of mtDNA transcription and maintenance system defects in the adult heart. Our novel $Tfam^{fl/flxMCM}$ model of inducible TFAM deletion in adult mouse cardiomyocytes revealed surprising contrasts to phenotypes observed with systemic TFAM deletion (embryonic lethality) (21) or myocardium-specific TFAM deletion in embryonic or early postnatal life (cardiomyopathy, shortened lifespan) (23, 24). Indeed, inactivating *Tfam* in adult mouse cardiomyocytes resulted in an unexpected and extended period of cardiac functional resilience, wherein mitochondrial function, mtDNA content, and cardiac ventricular performance were preserved despite the loss of TFAM protein. Although this functional resilience delayed disease onset, long-term deletion ultimately resulted in mitochondrial dysfunction and mitochondrial cardiomyopathy. These distinct phases of the cardiac response to TFAM inactivation illuminate unique features of adult heart mitochondria.

During functional resilience, although respiratory chain and cardiac performance were functionally indistinguishable between control and TFAM-null animals, key changes were induced by TFAM deletion. First, we observed derangements in mitochondrial organization in $Tfam^{fl/flxMCM}$ hearts at a time point when respiratory chain function was unchanged compared with $Tfam^{fl/fl}$ control mitochondria, suggesting that changes in mitochondrial morphology precede mitochondrial dysfunction. Interestingly, recent work with stimulated emission depletion nanoscopy of mitochondria revealed a highly ordered arrangement of mitochondrial nucleoids in relation to cristae, where nucleoids specifically occupy spaces separating groups of cristae (43). This finding suggests specific regulation underlying nucleoid-cristae positioning. In addition, within the nucleoid, TFAM interacts with mitofilin/Mic60, a critical component of the mitochondrial contact site and cristae organization system (MICOS) complex, which participates in cristae remodeling (44). Mitofilin deletion causes aberrant mitochondrial morphology with abnormal cristae structure and mtDNA depletion. Although the mechanisms of mitofilin deletion-mediated mtDNA loss are not fully understood and may involve defects in nucleoid segregation during organelle division, our observations of abnormal mitochondrial morphology in the absence of both TFAM protein and overt mitochondrial energetics defects supports a model of TFAM-dependent regulation of mitochondrial morphology in the adult heart.

In addition to TFAM-dependent changes in mitochondrial ultrastructure, functional resilience to TFAM inactivation in adult cardiomyocytes was also marked by the surprising ability of $Tfam^{fl/flxMCM}$ mitochondria to maintain normal levels of mitochondrial respiration and a striking disconnect between TFAM-dependent mtDNA transcription and mtDNA content. Extensive literature implicates TFAM as a transcription factor for mtDNA and regulator of mtDNA

Figure 2. Prolonged mitochondrial transcription factor A (TFAM) inactivation in adult cardiomyocytes causes a delayed-onset mitochondrial cardiomyopathy. Tamoxifen dosing and experimental time course for prolonged TFAM deletion (32 wk posttamoxifen). Representative images of 7-μm transverse heart sections from mice of the indicated genotypes at 32 wk posttamoxifen (*A*) stained with hematoxylin and eosin (H&E) (*B*). $Tfam^{fl/flxMCM}$ hearts display extensive inflammatory infiltrate. *C*: quantification of myocyte cross-sectional area from the indicated genotypes ($n = 3$ animals/group; >200 myocytes/animal evaluated). *D*: representative images of Masson's trichrome staining. $Tfam^{fl/flxMCM}$ hearts display increased fibrosis as compared with controls. HW/BW ratio ($n = 7$ fl/fl, $n = 8$ fl/flxMCM) (*E*), lung weight to body weight ratio (LW/BW; $n = 7$ fl/fl, $n = 8$ fl/flxMCM) (*F*), LVIDd ($n = 9$ fl/fl, $n = 6$ fl/flxMCM) (*G*), and fractional shortening (FS; $n = 9$ fl/fl, $n = 6$ fl/flxMCM) (*H*) assessed at the 32-wk post-tamoxifen time point. Real-time PCR (RT-PCR) analyses of *Nppa* (*I*), *Nppb* (*J*), and *Myh6* expression (n = 4/group) (*K*). All values reported as means ± SE. Student's *t* test was used for statistical analysis. $P < 0.05$ was considered significant. *$P < 0.05$, **$P < 0.01$, ***$P < 0.0005$, and ****$P < 0.0001$.

AJP-Cell Physiol • doi:10.1152/ajpcell.00508.2020 • www.ajpcell.org

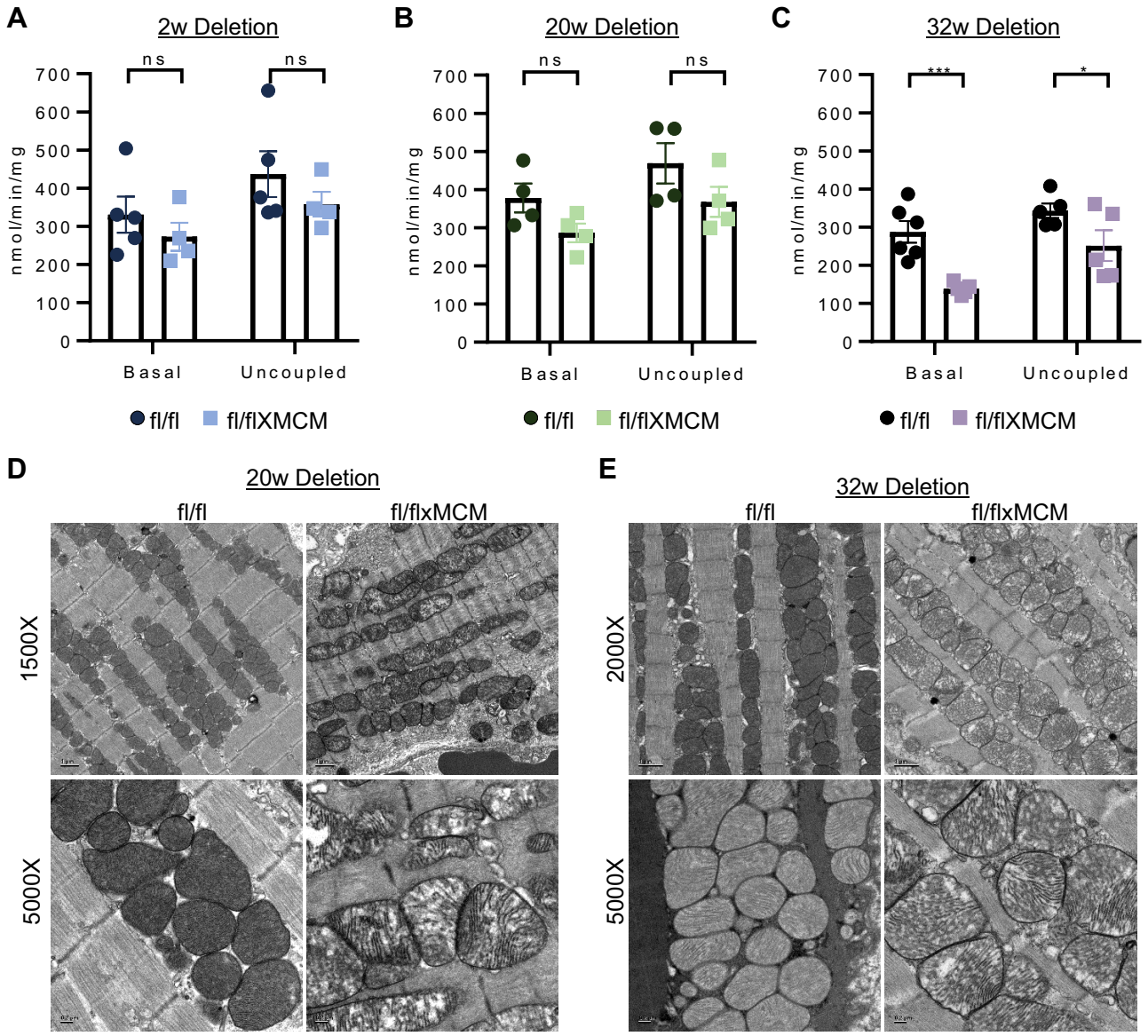

Figure 3. Mitochondrial transcription factor A (TFAM) deletion-induced mitochondrial remodeling precedes onset of mitochondrial dysfunction. Basal and uncoupled mitochondrial oxygen consumption rates measured in isolated cardiac mitochondria from *Tfam*$^{fl/fl}$ vs. *Tfam*$^{fl/flxMCM}$ mice at 2 wk ($n = 4$/group) (*A*), 20 wk ($n = 4$/group) (*B*), and 32 wk posttamoxifen ($n = 5$/group) (*C*). Representative electron micrographs of left ventricular ultrastructure from the genotypes indicated at 20 wk ($n = 3$ fl/fl and $n = 3$ fl/flxMCM animals analyzed) (*D*) and 32 wk posttamoxifen ($n = 2$ fl/fl and $n = 3$ fl/flxMCM animals analyzed) (*E*). All values presented as means ± SE. Student's *t* test was used for statistical analysis. $P < 0.05$ was considered significant. $^{*}P < 0.05$ and $^{***}P < 0.001$.

content (as transcription generates the RNA primer to initiate mtDNA replication) and mtDNA compaction. In vitro and in vivo, TFAM loss induces coincident decreases in mtDNA transcription and copy number; in contrast, in vivo TFAM overexpression produces increased mtDNA copy number (19). Yet, our study revealed that TFAM protein levels do not automatically determine mitochondrial genome abundance in the adult heart: during functional resilience, *Tfam*$^{fl/flxMCM}$ hearts displayed preserved cmtDNA content despite TFAM loss. In addition, studies of mtDNA turnover rates in rodent heart calculated mtDNA half-lives ranging from 6.7 days (45) to 350 days (46). Our data support a model of a longer turnover time in adult cardiomyocytes (47), which may allow for mitochondrial genome abundance to be preserved following TFAM deletion.

Because mtDNA replication initiation requires transcription-based priming, our observations of unchanged mtDNA levels and preserved mitochondrial function in *Tfam*$^{fl/flxMCM}$ cardiac mitochondria initially led us to hypothesize that mitochondrial transcription would be similarly unaltered. However, decreases in mitochondrial transcript levels in *Tfam*$^{fl/flxMCM}$ hearts were an early response following induction of TFAM inactivation (decreases in transcript levels observed as early as 2 wk posttamoxifen). Thus, acute deletion of TFAM in adult cardiomyocytes impairs mitochondrial transcription, and we postulate that mitochondrial translation—which was unchanged in *Tfam*-deleted versus

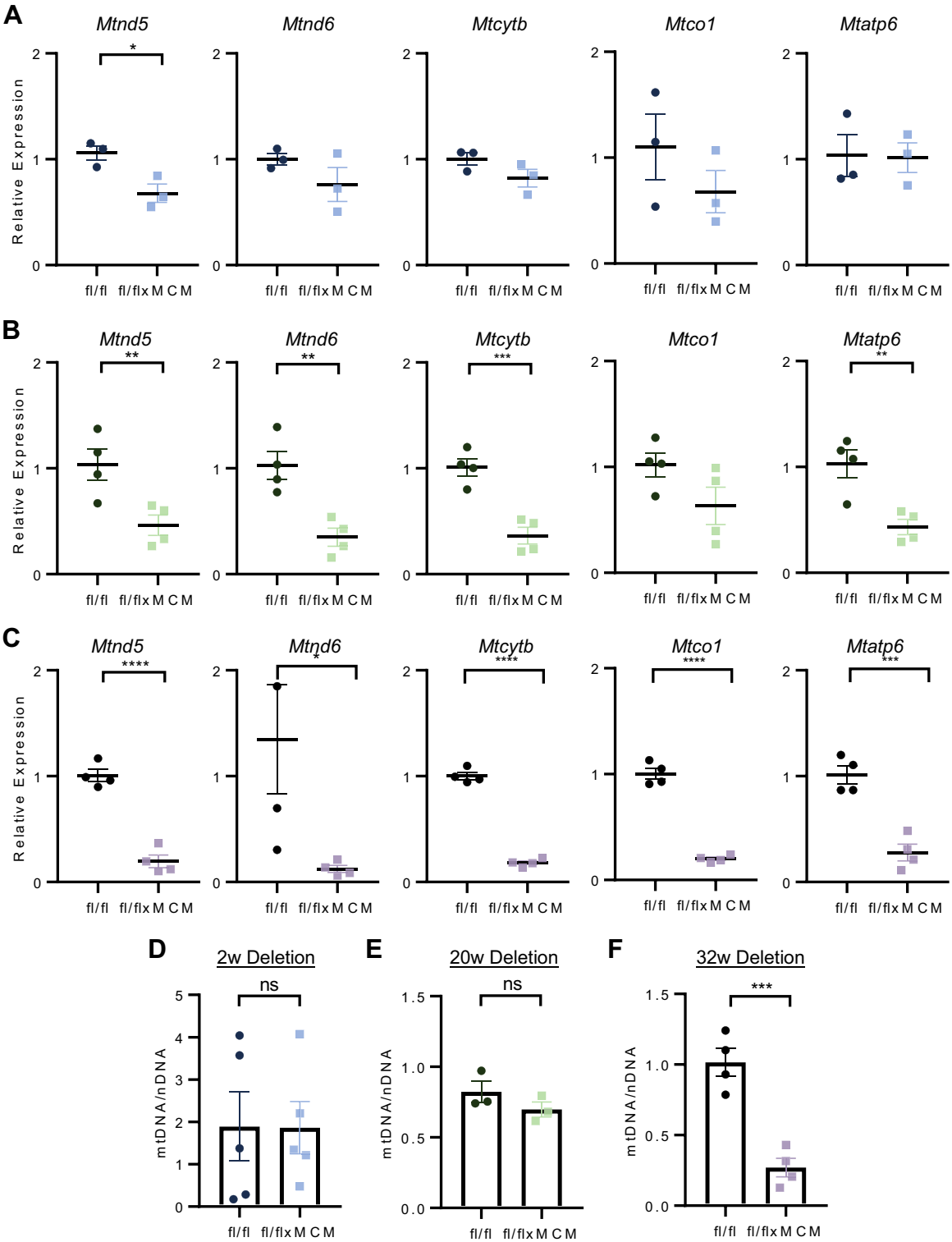

Figure 4. Defects in mitochondrial DNA (mtDNA) transcription are an early response to mitochondrial transcription factor A (TFAM) deletion. Real-time PCR (RT-PCR) analyses of steady state mtDNA-encoded transcript levels at 2- (*A*), 20- (*B*), and 32-wk (*C*) posttamoxifen ($n = 3$–4/group). Quantification of cardiac mtDNA to nuclear DNA (nDNA) ratios from animals at the 2- (*D*), 20- (*E*), and 32-wk (*F*) posttamoxifen time points ($n = 3$–5/group). Values presented as means ± SE. Student's *t* test was used for statistical analysis. $P < 0.05$ was considered significant. *$P < 0.05$, **$P < 0.01$, ***$P < 0.001$, ****$P < 0.0001$.

AJP-Cell Physiol • doi:10.1152/ajpcell.00508.2020 • www.ajpcell.org

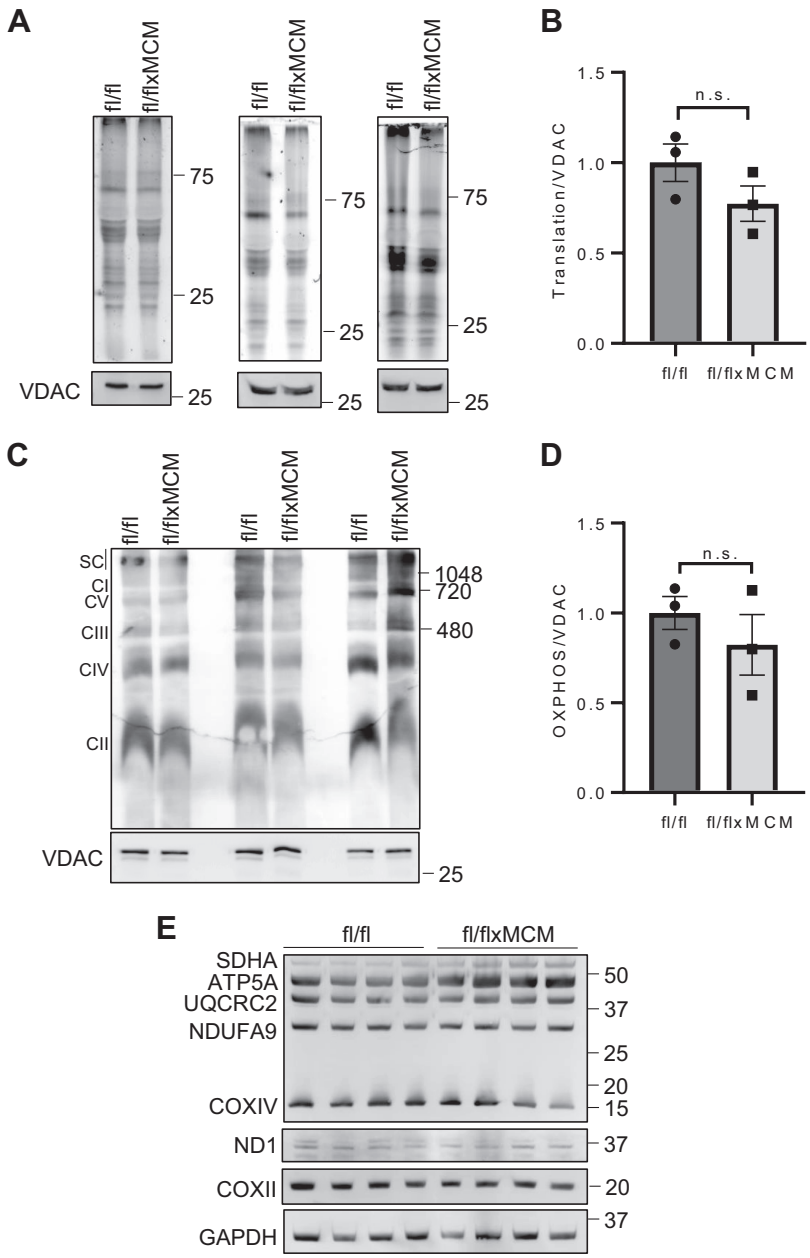

Figure 5. Mitochondrial protein translation is preserved during functional resilience. *A*: representative image of SDS-PAGE analyses of azidohomoalanine (AHA)-labeled proteins produced by in organello translation assays performed on cardiac mitochondria isolated from $Tfam^{fl/fl}$ and $Tfam^{fl/flxMCM}$ animals 13 wk following tamoxifen dosing (3 independent experiments shown). A Western blot for VDAC on the input mitochondria was used as a protein loading control. *B*: densitometry quantification of the in organello translation assays ($n = 3$/group). *C*: analyses of the respiratory chain complex abundance and assembly in cardiac mitochondria isolated from $Tfam^{fl/fl}$ and $Tfam^{fl/flxMCM}$ animals 13 wk post-tamoxifen. Mitochondrial proteins were resolved by blue-native polyacrylamide gel electrophoresis (BN-PAGE) followed by immunoblotting with the Total oxidative phosphorylation (OXPHOS) antibody cocktail to simultaneously visualize all five complexes of the respiratory chain. A Western blot for the voltage-dependent anion channel, VDAC, on the input mitochondria was used as a protein loading control. *D*: densitometry quantification of BN-PAGE ($n = 3$/group). Values presented as means ± SE. Student's *t* test was used for statistical analysis. *E*: Western blot of nDNA encoded (SDHA, ATP5A, UQCRC2, NDUFA9, and COXIV) and mitochondrial DNA (mtDNA encoded (ND1 and COXII) respiratory chain subunits in $Tfam^{fl/fl}$ ($n = 4$) vs. $Tfam^{fl/flxMCM}$ ($n = 4$) hearts. GAPDH was used as a protein loading control. TFAM, mitochondrial transcription factor A.

control mitochondria during functional resilience—contributes to maintaining mitochondrial function. Ultimately, $Tfam^{fl/flxMCM}$ mitochondrial function might be subject to threshold effects, whereby declining mitochondrial transcript levels due to *Tfam* inactivation may not manifest as impaired mitochondrial translation until total transcripts decrease below a certain level. As our data suggest that the mitochondrial RNA degradosome is unaltered with TFAM deletion, the findings may further support a model where transcript levels in cardiac mitochondria are in excess and mitochondrial translation serves as a response to sustain mitochondrial function in the face of acute defects to the mtDNA regulatory machinery (48).

How $Tfam^{fl/flxMCM}$ hearts transition from functional resilience to cardiomyopathy is perplexing, and complete delineation of this signaling pathway is beyond the scope of the present study. Our observations that PGC1α levels begin to decrease at the 20-wk deletion time point (the tail end of our functional resilience window), tracking with the onset of reduced nDNA-encoded respiratory chain subunits suggest that PGC1α-dependent alterations in mitochondrial genes may contribute to the transition to cardiac disease. However, we also found that long-term cardiomyocyte TFAM inactivation (32 wk posttamoxifen) downregulated the expression of the core mitochondrial transcription and mtDNA replication machinery. Interestingly, expression of these factors was unaltered during functional resilience (unaltered at the 20-

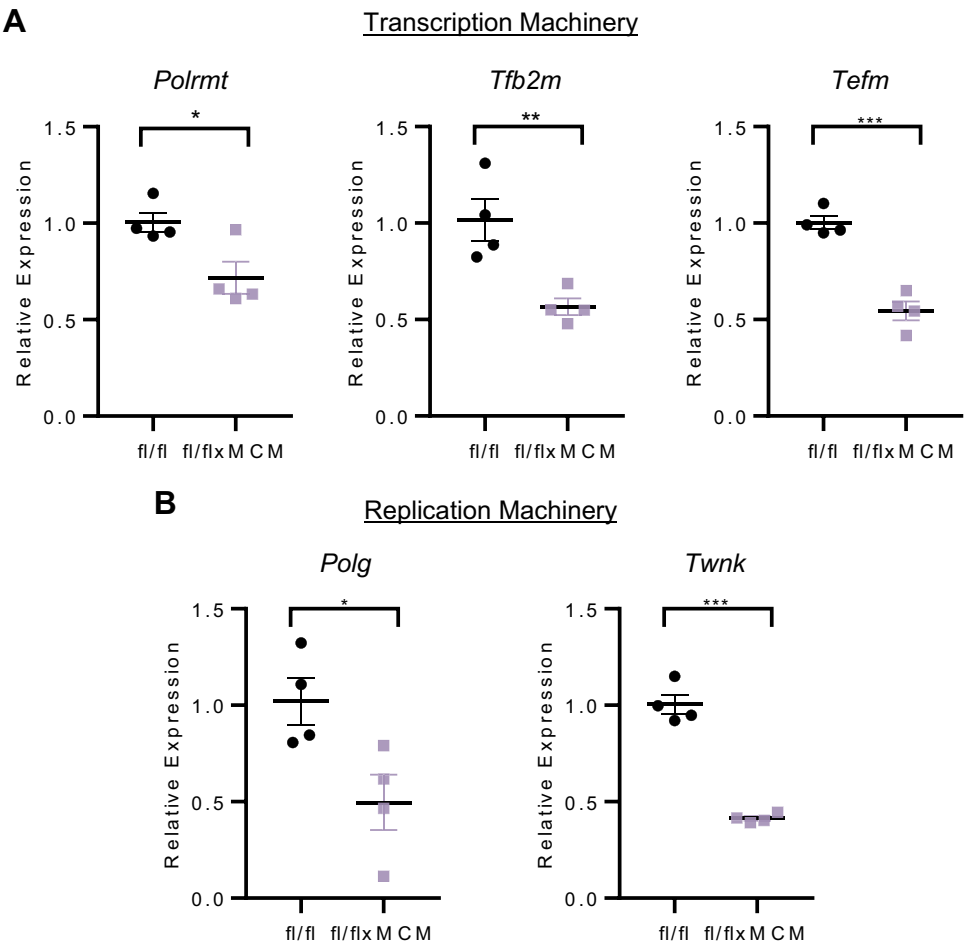

Figure 6. Downregulation of the mitochondrial DNA (mtDNA) transcription and replication machinery with prolonged mitochondrial transcription factor A (TFAM) loss. *A*: Real-time PCR (RT-PCR) analyses of components of the mtDNA transcription machinery (*Polrmt*, *Tfb2m*, *Tefm*). $n = 4$/group. *B*: RT-PCR analyses of components of the mtDNA replication machinery (*Polg* and *Twnk*). $n = 4$/group. Values presented as means ± SE. Student's *t* test was used for statistical analysis. $P < 0.05$ was considered significant. $^{*}P < 0.05$, $^{**}P < 0.01$, and $^{***}P < 0.001$.

wk deletion time point), suggesting that TFAM deletion-induced downregulation of the mitochondrial transcription and replication machinery is a specific feature of prolonged cardiomyocyte TFAM loss. Moreover, this temporal disconnect between the decline in nDNA-encoded respiratory chain transcripts versus transcripts encoding the mtDNA transcription and replication machinery suggests that reprogramming of the cardiac transcriptome in response to TFAM deletion is complex and may extend beyond PCG1α regulation. Ultimately, our results suggest that impaired mtDNA transcription and replication likely potentiates the decline in mitochondrial transcripts and genome abundance and may serve as a feed-forward mechanism underlying the mitochondrial and cardiac dysfunction observed with prolonged TFAM ablation.

In summary, we found that loss of TFAM elicits different effects on mtDNA transcription, replication, and maintenance systems in adult versus embryonic/postnatal hearts. Although initiating *Tfam* deletion at either life stage causes cardiomyopathy, the differences in timing of disease onset and development are striking. A possible explanation for these differences—early and rapid onset of cardiomyopathy and shortened lifespan in embryonic/postnatal mice, versus functional resilience and slow disease onset in adult—is the inherent differences between these two stages: the embryonic/postnatal heart is a developing tissue undergoing active growth and proliferation, whereas the adult heart is terminally differentiated. Metabolic requirements, mitochondrial function, and even mitochondrial morphology differ between these two states—with the more fragmented mitochondria of the developing cardiomyocytes maturing into a highly interconnected reticulum of the differentiated cardiomyocytes, (28, 49, 50). Moreover, TFAM may have a critical role in cardiomyocyte proliferation (22). Thus, it is possible that cells undergoing active growth and proliferation have a greater dependence on TFAM function and could require higher rates of TFAM-facilitated mtDNA transcription and synthesis than terminally-differentiated cardiomyocytes.

Taken together, our study highlights the need to delineate mitochondrial maintenance pathways in both developing and differentiated tissues and organ systems, particularly because mitochondrial dysfunction is implicated in aging and disease.

SUPPLEMENTAL DATA

Supplemental Figs. S1–S8: https://doi.org/10.6084/m9.figshare.14153687.

GRANTS

Electron microscopy for this study was supported by the Robert P. Apkarian Integrated Electron Microscopy Core (RPAIEMC), which

is subsidized by the Emory University School of Medicine and the Emory College of Arts and Sciences. Additional support for electron microscopy was provided by the Georgia Clinical & Translational Science Alliance of the National Institutes of Health under award number UL1TR000454. Echocardiography for this study was supported in part by the Animal Physiology Core, which is subsidized by Emory University and Children's Healthcare of Atlanta. Additional support was provided by the Office of the Director of the National Institutes of Health under Award Number S10OD021748. Histology for this study was supported in part by the Cancer Tissue and Pathology shared resource of Winship Cancer Institute of Emory University and NIH/NCI under award number P30CA138292.

DISCLOSURES

No conflicts of interest, financial or otherwise, are declared by the authors.

AUTHOR CONTRIBUTIONS

J.Q.K. conceived and designed research; N.G., J.N.P., and T.A.M. performed experiments; N.G., J.N.P., and J.Q.K. analyzed data; J.Q.K. interpreted results of experiments; N.G., J.N.P., and J.Q.K. prepared figures; J.Q.K. drafted manuscript; J.Q.K. edited and revised manuscript; N.G., J.N.P., T.A.M., and J.Q.K. approved final version of manuscript.

REFERENCES

1. **Harris DA**, **Das AM.** Control of mitochondrial ATP synthesis in the heart. *Biochem J* 280: 561–573, 1991. doi:10.1042/bj2800561.
2. **Page E**, **McCallister LP.** Quantitative electron microscopic description of heart muscle cells. Application to normal, hypertrophied and thyroxin-stimulated hearts. *Am J Cardiol* 31: 172–181, 1973. doi:10.1016/0002-9149(73)91030-8.
3. **Bates MG**, **Bourke JP**, **Giordano C**, **d'Amati G**, **Turnbull DM**, **Taylor RW.** Cardiac involvement in mitochondrial DNA disease: clinical spectrum, diagnosis, and management. *Eur Heart J* 33: 3023–3033, 2012. doi:10.1093/eurheartj/ehs275.
4. **Ide T**, **Tsutsui H**, **Hayashidani S**, **Kang D**, **Suematsu N**, **Nakamura K**, **Utsumi H**, **Hamasaki N**, **Takeshita A.** Mitochondrial DNA damage and dysfunction associated with oxidative stress in failing hearts after myocardial infarction. *Circ Res* 88: 529–535, 2001. doi:10.1161/01.res.88.5.529.
5. **Rosca MG**, **Hoppel CL.** Mitochondrial dysfunction in heart failure. *Heart Fail Rev* 18: 607–622, 2013. doi:10.1007/s10741-012-9340-0.
6. **Sugiyama S**, **Hattori K**, **Hayakawa M**, **Ozawa T.** Quantitative analysis of age-associated accumulation of mitochondrial DNA with deletion in human hearts. *Biochem Biophys Res Commun* 180: 894–899, 1991. doi:10.1016/s0006-291x(05)81149-0.
7. **Calvo SE**, **Mootha VK.** The mitochondrial proteome and human disease. *Annu Rev Genomics Hum Genet* 11: 25–44, 2010. doi:10.1146/annurev-genom-082509-141720.
8. **Anderson S**, **Bankier AT**, **Barrell BG**, **de Bruijn MH**, **Coulson AR**, **Drouin J**, **Eperon IC**, **Nierlich DP**, **Roe BA**, **Sanger F**, **Schreier PH**, **Smith AJ**, **Staden R**, **Young IG.** Sequence and organization of the human mitochondrial genome. *Nature* 290: 457–465, 1981. doi:10.1038/290457a0.
9. **Gilkerson R**, **Bravo L**, **Garcia I**, **Gaytan N**, **Herrera A**, **Maldonado A**, **Quintanilla B.** The mitochondrial nucleoid: integrating mitochondrial DNA into cellular homeostasis. *Cold Spring Harb Perspect Biol* 5: a011080, 2013. doi:10.1101/cshperspect.a011080.
10. **Bogenhagen DF**, **Rousseau D**, **Burke S.** The layered structure of human mitochondrial DNA nucleoids. *J Biol Chem* 283: 3665–3675, 2008. doi:10.1074/jbc.M708444200.
11. **Kaufman BA**, **Newman SM**, **Hallberg RL**, **Slaughter CA**, **Perlman PS**, **Butow RA.** In organello formaldehyde crosslinking of proteins to mtDNA: identification of bifunctional proteins. *Proc Natl Acad Sci USA* 97: 7772–7777, 2000. doi:10.1073/pnas.140063197.
12. **Rajala N**, **Hensen F**, **Wessels HJ**, **Ives D**, **Gloerich J**, **Spelbrink JN.** Whole cell formaldehyde cross-linking simplifies purification of mitochondrial nucleoids and associated proteins involved in mitochondrial gene expression. *PLoS One* 10: e0116726, 2015. doi:10.1371/journal.pone.0116726.
13. **Kaufman BA**, **Durisic N**, **Mativetsky JM**, **Costantino S**, **Hancock MA**, **Grutter P**, **Shoubridge EA.** The mitochondrial transcription factor TFAM coordinates the assembly of multiple DNA molecules into nucleoid-like structures. *Mol Biol Cell* 18: 3225–3236, 2007. doi:10.1091/mbc.e07-05-0404.
14. **Ngo HB**, **Kaiser JT**, **Chan DC.** The mitochondrial transcription and packaging factor Tfam imposes a U-turn on mitochondrial DNA. *Nat Struct Mol Biol* 18: 1290–1296, 2011. doi:10.1038/nsmb.2159.
15. **Ngo HB**, **Lovely GA**, **Phillips R**, **Chan DC.** Distinct structural features of TFAM drive mitochondrial DNA packaging versus transcriptional activation. *Nat Commun* 5: 3077, 2014. doi:10.1038/ncomms4077.
16. **Dairaghi DJ**, **Shadel GS**, **Clayton DA.** Human mitochondrial transcription factor A and promoter spacing integrity are required for transcription initiation. *Biochim Biophys Acta* 1271: 127–134, 1995. doi:10.1016/0925-4439(95)00019-Z.
17. **Shi Y**, **Dierckx A**, **Wanrooij PH**, **Wanrooij S**, **Larsson NG**, **Wilhelmsson LM**, **Falkenberg M**, **Gustafsson CM.** Mammalian transcription factor A is a core component of the mitochondrial transcription machinery. *Proc Natl Acad Sci USA* 109: 16510–16515, 2012. doi:10.1073/pnas.1119738109.
18. **Falkenberg M.** Mitochondrial DNA replication in mammalian cells: overview of the pathway. *Essays Biochem* 62: 287–296, 2018. doi:10.1042/EBC20170100.
19. **Ekstrand MI**, **Falkenberg M**, **Rantanen A**, **Park CB**, **Gaspari M**, **Hultenby K**, **Rustin P**, **Gustafsson CM**, **Larsson NG.** Mitochondrial transcription factor A regulates mtDNA copy number in mammals. *Hum Mol Genet* 13: 935–944, 2004. doi:10.1093/hmg/ddh109.
20. **Ikeda M**, **Ide T**, **Fujino T**, **Arai S**, **Saku K**, **Kakino T**, **Tyynismaa H**, **Yamasaki T**, **Yamada K**, **Kang D**, **Suomalainen A**, **Sunagawa K.** Overexpression of TFAM or twinkle increases mtDNA copy number and facilitates cardioprotection associated with limited mitochondrial oxidative stress. *PLoS One* 10: e0119687, 2015. doi:10.1371/journal.pone.0119687.
21. **Larsson NG**, **Wang J**, **Wilhelmsson H**, **Oldfors A**, **Rustin P**, **Lewandoski M**, **Barsh GS**, **Clayton DA.** Mitochondrial transcription factor A is necessary for mtDNA maintenance and embryogenesis in mice. *Nat Genet* 18: 231–236, 1998. doi:10.1038/ng0398-231.
22. **Zhang D**, **Li Y**, **Heims-Waldron D**, **Bezzerides V**, **Guatimosim S**, **Guo Y**, **Gu F**, **Zhou P**, **Lin Z**, **Ma Q**, **Liu J**, **Wang DZ**, **Pu WT.** Mitochondrial cardiomyopathy caused by elevated reactive oxygen species and impaired cardiomyocyte proliferation. *Circ Res* 122: 74–87, 2018. doi:10.1161/CIRCRESAHA.117.311349.
23. **Wang J**, **Wilhelmsson H**, **Graff C**, **Li H**, **Oldfors A**, **Rustin P**, **Bruning JC**, **Kahn CR**, **Clayton DA**, **Barsh GS**, **Thoren P**, **Larsson NG.** Dilated cardiomyopathy and atrioventricular conduction blocks induced by heart-specific inactivation of mitochondrial DNA gene expression. *Nat Genet* 21: 133–137, 1999. doi:10.1038/5089.
24. **Li H**, **Wang J**, **Wilhelmsson H**, **Hansson A**, **Thoren P**, **Duffy J**, **Rustin P**, **Larsson NG.** Genetic modification of survival in tissue-specific knockout mice with mitochondrial cardiomyopathy. *Proc Natl Acad Sci USA* 97: 3467–3472, 2000. doi:10.1073/pnas.97.7.3467.
25. **Sommakia S**, **Houlihan PR**, **Deane SS**, **Simcox JA**, **Torres NS**, **Jeong MY**, **Winge DR**, **Villanueva CJ**, **Chaudhuri D.** Mitochondrial cardiomyopathies feature increased uptake and diminished efflux of mitochondrial calcium. *J Mol Cell Cardiol* 113: 22–32, 2017. doi:10.1016/j.yjmcc.2017.09.009.
26. **Yutzey KE.** Cardiomyocyte proliferation: teaching an old dogma new tricks. *Circ Res* 120: 627–629, 2017. doi:10.1161/CIRCRESAHA.116.310058.
27. **Karbassi E**, **Fenix A**, **Marchiano S**, **Muraoka N**, **Nakamura K**, **Yang X**, **Murry CE.** Cardiomyocyte maturation: advances in knowledge and implications for regenerative medicine. *Nat Rev Cardiol* 17: 341–359, 2020. doi:10.1038/s41569-019-0331-x.
28. **Piquereau J**, **Ventura-Clapier R.** Maturation of cardiac energy metabolism during perinatal development. *Front Physiol* 9: 959, 2018. doi:10.3389/fphys.2018.00959.
29. **Agah R**, **Frenkel PA**, **French BA**, **Michael LH**, **Overbeek PA**, **Schneider MD.** Gene recombination in postmitotic cells. Targeted expression of Cre recombinase provokes cardiac-restricted, site-

specific rearrangement in adult ventricular muscle in vivo. *J Clin Invest* 100: 169–179, 1997. doi:10.1172/JCI119509.

30. **Sohal DS**, **Nghiem M**, **Crackower MA**, **Witt SA**, **Kimball TR**, **Tymitz KM**, **Penninger JM**, **Molkentin JD.** Temporally regulated and tissue-specific gene manipulations in the adult and embryonic heart using a tamoxifen-inducible Cre protein. *Circ Res* 89: 20–25, 2001. doi:10.1161/hh1301.092687.
31. **Goonasekera SA**, **Hammer K**, **Auger-Messier M**, **Bodi I**, **Chen X**, **Zhang H**, **Reiken S**, **Elrod JW**, **Correll RN**, **York AJ**, **Sargent MA**, **Hofmann F**, **Moosmang S**, **Marks AR**, **Houser SR**, **Bers DM**, **Molkentin JD.** Decreased cardiac L-type Ca(2)(+) channel activity induces hypertrophy and heart failure in mice. *J Clin Invest* 122: 280–290, 2012. doi:10.1172/JCI58227.
32. **Malik AN**, **Czajka A**, **Cunningham P.** Accurate quantification of mouse mitochondrial DNA without co-amplification of nuclear mitochondrial insertion sequences. *Mitochondrion* 29: 59–64, 2016. doi:10.1016/j.mito.2016.05.003.
33. **Spandidos A**, **Wang X**, **Wang H**, **Seed B.** PrimerBank: a resource of human and mouse PCR primer pairs for gene expression detection and quantification. *Nucleic Acids Res* 38: D792–D799, 2010. doi:10.1093/nar/gkp1005.
34. **Ahuja M**, **Ammal Kaidery N**, **Yang L**, **Calingasan N**, **Smirnova N**, **Gaisin A**, **Gaisina IN**, **Gazaryan I**, **Hushpulian DM**, **Kaddour-Djebbar I**, **Bollag WB**, **Morgan JC**, **Ratan RR**, **Starkov AA**, **Beal MF**, **Thomas B.** Distinct Nrf2 signaling mechanisms of fumaric acid esters and their role in neuroprotection against 1-methyl-4-phenyl-1,2,3,6-tetrahydropyridine-induced experimental Parkinson's-like disease. *J Neurosci* 36: 6332–6351, 2016. doi:10.1523/JNEUROSCI.0426-16.2016.
35. **Kwong JQ**, **Davis J**, **Baines CP**, **Sargent MA**, **Karch J**, **Wang X**, **Huang T**, **Molkentin JD.** Genetic deletion of the mitochondrial phosphate carrier desensitizes the mitochondrial permeability transition pore and causes cardiomyopathy. *Cell Death Differ* 21: 1209–1217, 2014. doi:10.1038/cdd.2014.36.
36. **Kwong JQ**, **Lu X**, **Correll RN**, **Schwanekamp JA**, **Vagnozzi RJ**, **Sargent MA**, **York AJ**, **Zhang J**, **Bers DM**, **Molkentin JD.** The mitochondrial calcium uniporter selectively matches metabolic output to acute contractile stress in the heart. *Cell Rep* 12: 15–22, 2015. doi:10.1016/j.celrep.2015.06.002.
37. **Fernandez-Silva P**, **Acin-Perez R**, **Fernandez-Vizarra E**, **Perez-Martos A**, **Enriquez JA.** In vivo and in organello analyses of mitochondrial translation. *Methods Cell Biol* 80: 571–588, 2007. doi:10.1016/S0091-679X(06)80028-2.
38. **Jha P**, **Wang X**, **Auwerx J.** Analysis of mitochondrial respiratory chain supercomplexes using blue native polyacrylamide gel electrophoresis (BN-PAGE). *Curr Protoc Mouse Biol* 6: 1–14, 2016. doi:10.1002/9780470942390.mo150182.
39. **Wittig I**, **Braun HP**, **Schagger H.** Blue native PAGE. *Nat Protoc* 1: 418–428, 2006. doi:10.1038/nprot.2006.62.
40. **Borowski LS**, **Dziembowski A**, **Hejnowicz MS**, **Stepien PP**, **Szczesny RJ.** Human mitochondrial RNA decay mediated by PNPase-hSuv3 complex takes place in distinct foci. *Nucleic Acids Res* 41: 1223–1240, 2013. doi:10.1093/nar/gks1130.
41. **Ventura-Clapier R**, **Garnier A**, **Veksler V.** Transcriptional control of mitochondrial biogenesis: the central role of PGC-1alpha. *Cardiovasc Res* 79: 208–217, 2008. doi:10.1093/cvr/cvn098.
42. **Barshad G**, **Marom S**, **Cohen T**, **Mishmar D.** Mitochondrial DNA transcription and its regulation: an evolutionary perspective. *Trends Genet* 34: 682–692, 2018. doi:10.1016/j.tig.2018.05.009.
43. **Stephan T**, **Roesch A**, **Riedel D**, **Jakobs S.** Live-cell STED nanoscopy of mitochondrial cristae. *Sci Rep* 9: 12419, 2019. doi:10.1038/s41598-019-48838-2.
44. **Yang RF**, **Sun LH**, **Zhang R**, **Zhang Y**, **Luo YX**, **Zheng W**, **Zhang ZQ**, **Chen HZ**, **Liu DP.** Suppression of Mic60 compromises mitochondrial transcription and oxidative phosphorylation. *Sci Rep* 5: 7990, 2015. doi:10.1038/srep07990.
45. **Gross NJ**, **Getz GS**, **Rabinowitz M.** Apparent turnover of mitochondrial deoxyribonucleic acid and mitochondrial phospholipids in the tissues of the rat. *J Biol Chem* 244: 1552–1562, 1969. doi:10.1016/S0021-9258(18)91795-3.
46. **Collins ML**, **Eng S**, **Hoh R**, **Hellerstein MK.** Measurement of mitochondrial DNA synthesis in vivo using a stable isotope-mass spectrometric technique. *J Appl Physiol (1985)* 94: 2203–2211, 2003. doi:10.1152/japplphysiol.00691.2002.
47. **Poovathingal SK**, **Gruber J**, **Lakshmanan L**, **Halliwell B**, **Gunawan R.** Is mitochondrial DNA turnover slower than commonly assumed? *Biogerontology* 13: 557–564, 2012. doi:10.1007/s10522-012-9390-7.
48. **Lagouge M**, **Mourier A**, **Lee HJ**, **Spahr H**, **Wai T**, **Kukat C**, **Silva Ramos E**, **Motori E**, **Busch JD**, **Siira S**, **German Mouse Clinic C**, **Kremmer E**, **Filipovska A**, **Larsson NG**; **German Mouse Clinic Consortium.** SLIRP regulates the rate of mitochondrial protein synthesis and protects LRPPRC from degradation. *PLoS Genet* 11: e1005423, 2015. doi:10.1371/journal.pgen.1005423.
49. **Glancy B**, **Hartnell LM**, **Combs CA**, **Femnou A**, **Sun J**, **Murphy E**, **Subramaniam S**, **Balaban RS.** Power grid protection of the muscle mitochondrial reticulum. *Cell Rep* 19: 487–496, 2017 [Erratum in *Cell Rep* 23: 2832, 2018]. doi:10.1016/j.celrep.2017.03.063.
50. **Hom JR**, **Quintanilla RA**, **Hoffman DL**, **de Mesy Bentley KL**, **Molkentin JD**, **Sheu SS**, **Porter GA. Jr.**,The permeability transition pore controls cardiac mitochondrial maturation and myocyte differentiation**.** *Dev Cell* 21: 469–478, 2011 [Erratum in *Dev Cell* 21: 975, 2011]. doi:10.1016/j.devcel.2011.08.008.